ISSN 2616-5880 Vol. 6, Issue 2: 63-72, DOI: 10.25236/AJMC.2025.060209

Numerical Study on Flow and Heat Transfer in Bionic Bifurcated Microchannels with Gradient Porous Wall

Xinyu Shi[1,a,*], Wanting Hu[1,b], Chenhao Li[1], Jianing Jiang[1]

[1]*College of Science, China Jiliang University, Hangzhou, China*
[a]*shixinyu0604@163.com*, [b]*p23080854014@cjlu.edu.cn*

Abstract: *The bifurcated microchannel heat sinks (MCHS) have garnered significant attention owing to their advantages of a large heat transfer area, compact design, and reduced operating costs. And the gradient porous material (GPM) has been widely applied in enhanced heat transfer applications due to its flexibly designable structure, higher thermal conductivity and better stability. Therefore, a three-dimensional numerical model for bifurcated MCHS with gradient porous walls is established, in order to improve the thermal performance. Six porosity gradient configurations with the same pore size and average porosity are proposed. The effects of porosity arrangement, different inlet velocity and porosity gradient difference on the flow and heat transfer properties of MCHS were numerically analyzed. The results indicated that the design with small porosity near the bottom wall and large porosity near the top of the bifurcated MCHS contributes to enhancing the overall performance. Where, the Nusselt number of 3SIP is the largest, which increases by 12.4% compared with the UP. A comprehensive performance evaluation factor (PEF) was introduced to analyze the thermal and hydraulic performance of bifurcated MCHS, where the 2SIP has the best comprehensive performance and the PEF factor increases by 15.9% compared with the UP. The results of this study improve the heat transfer performance of MCHS, and promote the application of gradient porous materials and other enhanced heat transfer means for composite heat transfer.*

Keywords: *microchannel heat sinks, gradient porous material, fractal, fluid flow, heat transfer, numerical simulation*

1. Introduction

With the increasing integration of electronic devices, the demand for effective heat dissipation solutions in micro-electronic devices is progressively rising. Studies have demonstrated that employing enhanced heat transfer techniques can significantly improve the reliability of micro-electronic devices [1,2]. Traditional enhanced heat transfer techniques usually add a vent in microelectronic devices to improve the relative flow between the device and the cooling fluid. However, this method increases the size and cost of the device while enhancing heat transfer [3]. Therefore, traditional cooling methods are unable to satisfy the heat transfer requirements of integrated electronic devices. The microchannel heat sinks (MCHS), introduced by Tuckerman and Pease [4,5], has garnered significant attention owing to its advantages of a large heat transfer area, compact structure, and reduced operating costs.

In the past, most studies have concentrated on traditional microchannel designs, including parallel structures, serpentine configurations and so on. Nevertheless, they have some issues, such as high pressure drops, non-uniform heat dissipation, and inadequate heat transfer efficiency. The bionic bifurcation network offers a novel approach to the structural design of MCHS, with its superior heat transfer capacity and minimal pressure drop [6-8]. It can significantly enhance the heat and mass transfer efficiency of MCHS. Senn et al. [9] numerically investigated the flow and heat transfer performance of tree shaped bifurcate MCHS under laminar flow conditions. They found that the fractal bifurcation structure can effectively improve the heat transfer efficiency which has significantly higher convective heat transfer coefficient and lower pressure drop than the serpentine structure. Wang et al. [10] employed computational fluid dynamics (CFD) to investigate the impact of the bifurcation angle on the overall characteristics of the bifurcate MCHS. The results indicate that the bifurcation angle significantly influences the cooling performance of the network. Moreover, an increase in the bifurcation angle leads to a more substantial pressure drop. Inspired by the vein structure, Peng et al. [11] developed a novel wick vein fractal structure in MCHS. They demonstrated that this design can reduce transport resistance

ISSN 2616-5880 Vol. 6, Issue 2: 63-72, DOI: 10.25236/AJMC.2025.060209

by increasing the contact area, thereby owing better efficiency and performance compared with the traditional parallel structure. Xia et al. [12] incorporated a fractal bifurcated network into the cooling system of the main shaft and numerical analyzed its thermal and pressure drop characteristics. They indicated that the tree-shaped MCHS optimized the overall performance coefficient, while also achieving a more uniform temperature distribution and reducing the pressure drop. Zhang et al. [13] designed and systematically compared the thermal performance of three structures embedded in high-power microprocessors: the parallel structure, the self-similar fractal structure, and the tree fractal structure. The results indicated that the tree fractal structure exhibits superior overall thermal performance. Fang et al. [14] employed CFD to demonstrate that a MCHS with a three-layer fractal structure exhibits lower flow resistance and a more uniform temperature distribution compared to a single-layer structure.

Gradient porous material (GPM) is a type of porous material characterized by a heterogeneous microstructure[15]. In contrast to traditionally uniform porous material (UPM), GPM exhibit enhanced properties such as high stiffness, superior stability, excellent environmental adaptability, and versatile design capabilities [16]. As a result, it has garnered significant attention in recent years as a promising material for improving heat transfer performance. Hu et al. [17] generated a single pore structure based on a body-centered cubic structure to examine the impact of forward and reverse gradient changes in porosity on the melting time and average thermal storage rate of phase change material(PCM). The results indicated that the complete melting time of the gradient structure with an increasing porosity along the heat flow direction is 2.6% and 15.5% shorter compared to the uniform structure and gradient structure with a decreasing porosity gradient, respectively. Gao et al. [18] conducted both experiment and numerical simulation on a radial GPM in oil storage tanks. The results demonstrated that the gradient structure promotes natural convection between the layers, leading to an accelerated melting process compared to the uniform structure. Kang et al. [19] adjusted the compression degree of the bipolar plates in the polymer electrolyte membrane fuel cell to form a GPM in order to improve the robustness, steadiness, and air efficiency of fuel cells. The results revealed that the metal foam with a decreasing porosity gradient along the diagonal direction from the inlet to the outlet can increase the power of the fuel cell by 8.23% compared with the conventional metal foam. Li et al. [20] proposed an adsorption bed filled with GPM to improve the heat and mass transfer during adsorption refrigeration. And they suggested that the GPM bed with the porosity increasing from the cooling side to the steam side performs better in the adsorption rate and specific cooling power. Xu et al. [21] conducted an experimental study on the characteristics of boiling heat transfer using GPM with a constant porosity of 0.98 and varied PPI. They found that the Cu-Ni GPM performs better than that of Ni-Ni GPM when the heat flow density is low, however, this trend is reversed as the heat flow density increases because the excessively crowded bubbles in the Cu-Ni GPM lead to a decrease in heat transfer performance.

The above review indicates that employing an enhanced MCHS structure and novel porous materials can substantially improve the heat transfer performance of the device. However, research on the combined effects of GPM and bifurcated MCHS on thermal properties remains scarce. In order to further enhance the thermal capability of microelectronic devices, this study investigates the integration of bifurcated MCHS with GPM. A three-dimensional numerical model of bifurcated MCHS with gradient porosity walls is established, and their thermal and mass transfer characteristics are systematically analyzed. The impacts of the gradient porosity structure, inlet velocity, and porosity gradient difference on the performance of bifurcated MCHS were systematically analyzed and discussed. This study provides valuable guidance for the new design of MCHS and further enhances its heat and mass transfer performance as well as thermal management efficiency.

2. Mathematical Modelling

2.1 Physical Model

In this study, we employed an idealized T-type bifurcated network with a bifurcation order of k = 3. The structural diagram is presented in Figure 1(a). During the construction process, factors such as network wall thickness, symmetry, and structural distribution, among other complex influences, are disregarded. The dimensions of the model are L = 37.5 mm in length and H = 1.5 mm in height. In order to more accurately describe the structural characteristics of fractal bifurcation networks, this study introduces the scale factors α, β, and γ [22]:

$$l_k = l_0 \alpha^k \tag{1}$$

$$d_k = d_0 \beta^k \tag{2}$$

$$tp_k = tp_0\gamma^k \tag{3}$$

Where α and β represent the length ratio and diameter ratio of the network, respectively, and γ denotes the thickness ratio of the gradient porosity wall of the network. The β and γ are maintained at a constant value of 0.749, while α is fixed at 0.552 [23]. And d_k, l_k, and tp_k denotes the diameters, lengths, and gradient porosity wall thicknesses of fractal bifurcation channels. They adhere to the self-similar fractal characteristics defined by equations (1), (2), and (3). Due to the symmetric characteristics between channels, the research object can be simplified to the computational domain illustrated in Figure 1(b). The specific dimensional parameters for each stage are presented in Table 1.

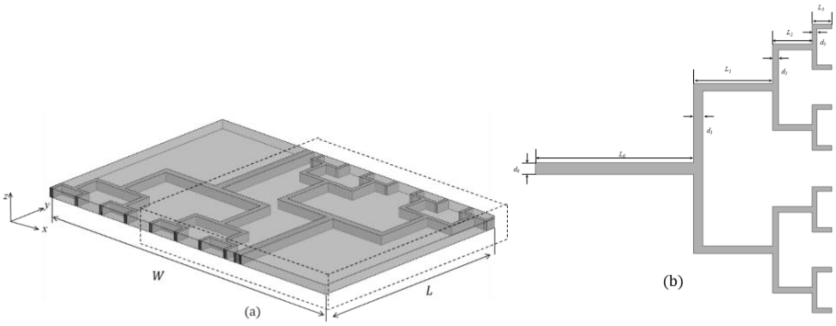

Fig. 1 (a) Geometric structure of bifurcated MCHS with gradient porosity walls; (b) Calculation domain diagram

Table 1. The parameters of bifurcated microchannels and graded porosity walls

Argument	k	**β=0.749**	**α=0.552**	**γ=0.749**
		d_k(mm)	l_k(mm)	tp_k(mm)
Bifurcation level	0	1.500	20	3.5
	1	1.191	10	2.62
	2	0.946	5	1.96
	3	0.751	2.5	1.47

As illustrated in Figure 2, six novel porous wall featuring gradient variations in porosity perpendicular to the flow direction were designed and implemented on both sides of the MCHS walls.

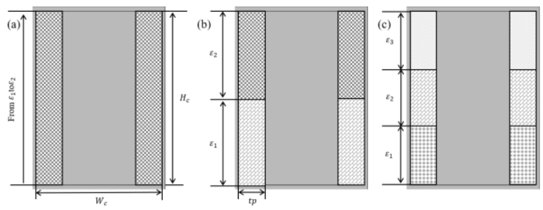

Fig. 2 (a) Linear variation; (b) two-layer variation; (c) three-layer variation

2.2 Mathematical model

The porous material is defined as Aluminum 6063-T83, the substrate material is specified as Aluminum 3003-H18, and the working fluid is water. The detailed physical properties of these materials are presented in Table 2. In order to analyze the fluid flow and heat transfer performance in a bifurcated MCHS with gradient porosity walls, the following assumptions are established: (1) The fluid is assumed to be in an incompressible flow state under steady state and laminar flow conditions. (2) The physical properties of the solid channels, porous walls, and fluids are considered independent of temperature. (3) The porous material within the wall is fully saturated, exhibits uniform properties, isotropic, and maintains local thermal equilibrium(LTE) [24] with the cooling fluid. (4) The Forchheimer-Brinkman-Darcy equation [25] is employed to characterize the fluid flow within the gradient porous wall. (5)The effects of gravity, heat transfer due to radiation, viscous dissipation, and other factors are neglected. (6) The deformation of the gradient porous media induced by heat in the walls is considered negligible.

Based on the above assumptions, the heat transfer and flow characteristics of the model can be determined by solving the continuity equations, momentum equations, and energy equations [26].

For fluids in gradient porous walls:

$$\nabla \cdot (\varepsilon \rho_f \vec{u}) = 0 \tag{4}$$

$$\frac{\rho_f}{\varepsilon^2}(\vec{u} \cdot \nabla)\vec{u} = -\nabla p + \frac{\mu_f}{\varepsilon}\nabla^2 \vec{u} - (\frac{\mu_f}{K} + \frac{\rho_f C_F}{\sqrt{K}}\left|\vec{u}\right|\vec{u}) \tag{5}$$

$$\rho_f C_{p,f}(\vec{u} \cdot \nabla T) = \lambda_{eff} \nabla^2 T \tag{6}$$

For fluids in channels outside of gradient porous walls:

$$\nabla \cdot (\rho_f \vec{u}) = 0 \tag{7}$$

$$\rho_f (\vec{u} \cdot \nabla)\vec{u} = -\nabla p + \mu_f \nabla^2 \vec{u} \tag{8}$$

$$\rho_f C_{p,f}(\vec{u} \cdot \nabla T) = \lambda_f \nabla^2 T \tag{9}$$

Where $\vec{u}$ is the velocity vector, ρ_f is the density, $C_{p,f}$ is the specific heat capacity, p is the pressure, and T is the temperature of the fluid in the calculation. Assuming that the porous material is composed of spherical particles, the permeability coefficient K was calculated by Ergun empirical equation [27]. And the inertia coefficient C_F and effective thermal conductivity λ_{eff} can be calculated by:

$$K = \frac{{d_p}^2 \varepsilon^3}{150(1-\varepsilon)^2} \tag{10}$$

$$C_F = \frac{3.5(1-\varepsilon)}{\varepsilon^3 d_p} \tag{11}$$

$$\lambda_{eff} = \varepsilon \lambda_f + (1-\varepsilon)\lambda_s \tag{12}$$

Where λ_f is the thermal conductivity of the fluid and λ_s is the thermal conductivity of the solid in gradient porous wall. The boundary conditions of the computational domain are defined as follows:

Inlet ($x=0$): $u = u_{in}, v = 0, w = 0, T_{in} = const$, Outlet ($x = L$): $p = 0$, Fluid-solid wall interfaces: $u = v = w = 0, T_s = T_f, k_s \nabla T_s = k_f \nabla T_f$;

Fluid-gradient porous wall interfaces: $u_p = u_f, v_p = v_f, w_p = w_f, T_p = T_f, k_{eff} \nabla T_p = k_f \nabla T_f$, Bottom wall of bifurcated microchannel: $q = const$ All interfaces except for the bottom wall and the outer wall: $\nabla T_{s|n} = 0$, where n is the normal unit vector of relevant surfaces.

Table 2. Physical properties of the working fluid and solid

Materials	$\rho(\mathrm{kg/m^3})$	$C_p(\mathrm{J/kg \cdot K})$	$\lambda = (\mathrm{W/m \cdot K})$	$\mu(\mathrm{Pa \cdot s})$
Aluminum 3003-H18	2730	893	155	—
Aluminum 6063-T83	2700	900	201	
Water	1000	4182	0.6	8.55×10^{-4}

2.3 Parameter definition

The Nusselt number (*Nu*), local thermal resistance (R_L), and total thermal resistance (R_T) are employed as key parameters to quantify the thermal characteristics of bifurcated microchannels:

$$Nu = \bar{h} D_h / \lambda_f \tag{13}$$

$$R_L = \frac{T_b - T_{\min}}{qA} \tag{14}$$

$$R_T = \frac{T_{\max} - T_{\min}}{qA} \tag{15}$$

ISSN 2616-5880 Vol. 6, Issue 2: 63-72, DOI: 10.25236/AJMC.2025.060209

where $\bar{h} = q_{in} / (T_w - T_f)$ is the convective heat transfer coefficient of the heat sink, $T_{\max}$, $T_{\min}$ and T_b are the maximum, minimum and the local temperature of the bottom surface of the bifurcated microchannel, respectively. A is the bottom area of the bifurcated microchannel.

Assessment of flow performance through pressure drop in bifurcated microchannels:

$$\Delta p = p_{in} - p_{out} \tag{16}$$

Where p_{in} and p_{out} are the inlet pressure and outlet pressure of the microchannel respectively.

The overall thermal performance of the microchannel was evaluated by the Comprehensive Performance Evaluation Factor (PEF):

$$\text{PEF} = \frac{Nu_i / Nu_0}{(f_i / f_0)^{1/3}} \tag{17}$$

Where, the subscript i denotes the parameters corresponding to gradient porous walls with varying structures, while the subscript 0 denotes the parameters associated with porous walls of uniform porosity.

2.4 Model validation

In this study, the CFD module in COMSOL Multiphysics was employed to solve the proposed control equations. These equations were discretized using the finite element method and solved with a double-precision solver. The second-order implicit pressure-link equation (SIMPLE) algorithm was employed to numerically solve the pressure-velocity coupling model using the PARDISO direct solver. The solver in the model is configured for three-dimensional, steady-state analysis, and multi-physics field coupling calculations are performed using the solid and fluid heat transfer module along with the laminar flow module. By defining an analytical function, the porosity of the porous wall is set to gradient vary along the z direction with linearly, two-layer and three-layer. To minimize reduce resources and time expenditure while maintaining model calculation accuracy, a grid independence test was conducted on four types of grids with varying thicknesses. Figure 3 illustrates the temperature distribution along the bottom wall of a channel under four different mesh density configurations. It can be clearly observed with mesh encryption, the maximum difference in the bottom wall temperature of the channel is less than 1.2%. Consequently, Grid3 (954982) has been selected for the calculation.

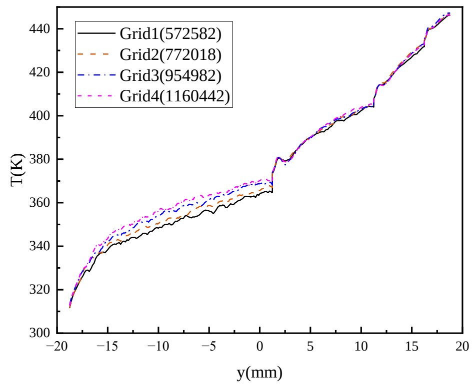

Fig. 3 Temperature distribution of a bifurcated microchannel under various mesh densities

In order to validate the numerical method and mathematical model employed in the calculation process, the simulation approach presented in this paper was utilized to construct an identical experiment model as that proposed by Dammel et al. Under the condition of a fixed external heat source of 175W, the bottom microchannel wall temperature was measured and compared with the data for inlet mass flow rates of 0.1 kg/min and 0.4 kg/min. It can be found in Fig 4, the maximum error between the numerical simulation results and the experimental results is 0.87% and 0.53% under the working condition of 0.1kg/min and 0.4 kg/min. Thus, the validity of the numerical method proposed in this chapter is successfully demonstrated.

ISSN 2616-5880 Vol. 6, Issue 2: 63-72, DOI: 10.25236/AJMC.2025.060209

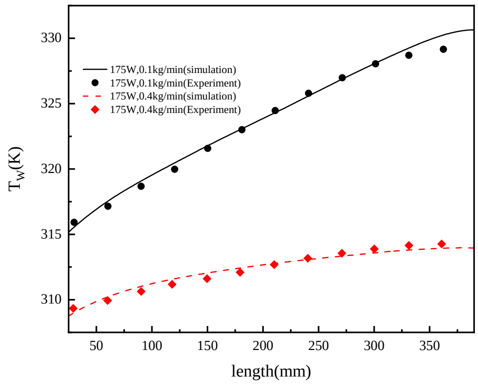

Fig. 4 The comparison of numerical average temperature with experimental data.

3. Results and discussion

3.1 Influence of different porosity structures

As depicted in Figure 5(a), six distinct gradient porous structures were designed and positioned on the inner walls of both sides of the bifurcated microchannel. The porosity of these structures varied gradually within the range of 0.75 to 0.95. They include two-layer porosity step increase (2SIP), two-layer porosity step decrease (2SDP), three-layer porosity step increase (3SIP), three-layer porosity step decrease (3SDP), linear porosity increase (LIP), linear porosity decrease (LDP), and are compared with the uniform porosity structure (UP).

Figure 5(b) illustrates the variation of local thermal resistance along one side of the flow path when gradient porous walls with different structures, under conditions of a constant pore size(0.1 mm), T_{in} = 300 K, and u_{in} = 0.2 m/s. As shown in Fig. 5(b), the local thermal resistance increases as the flow distance increases, and the local temperature of the bottom wall rises sharply near the bifurcation along the flow direction. This is because in a bifurcated microchannel, when the fluid flows from the main channel into the bifurcated channel, the alteration in flow direction induces changes in the boundary layer. This leads to a reduction in fluid velocity and the formation of eddy currents, thereby increasing the wall temperature. It can also found that the local thermal resistance of the porosity increasing structures is lower than that of the porosity decreasing structures and the uniform structure.

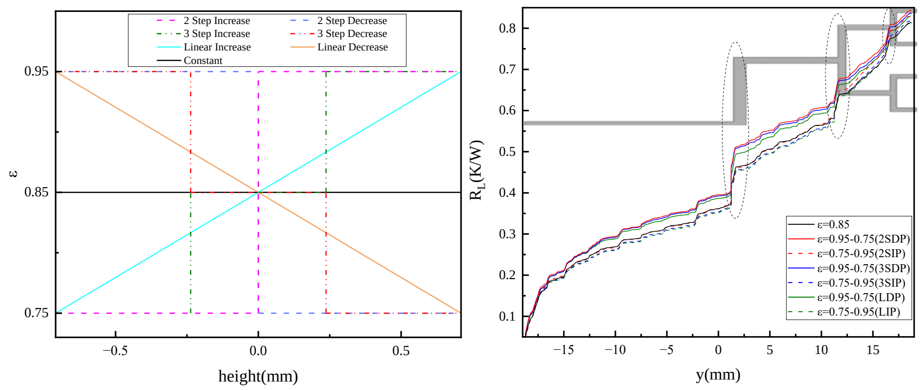

Fig. 5 (a) Different designs of porosity gradients; (b) Variation in local thermal resistance along the flow path within a single channel

Fig. 6 presents the velocity distribution at the interface between the gradient porosity wall and the channel cavity in a bifurcated microchannel. It can be found that the velocity is higher at levels 0 and 1 but has diminished at levels 2 and 3. Simultaneously, at levels 0 and 1, the velocity of different structures exhibit significant differences. In contrast, at levels 2 and 3, the velocity distributions of DP and IP structures are relatively similar, with less noticeable variation. This is because, as the bifurcation series of the channel increases, the fluid generates additional resistance when altering its flow direction at the bifurcations. It leads to a continuous reduction in fluid velocity and the less pronounced impact of varying porosity gradient structure designs on its velocity distribution. As shown in Fig. 6(a) and (b), it is evident that the velocity profiles of the 2SDP and 2SIP structures exhibit significant abrupt changes and

ISSN 2616-5880 Vol. 6, Issue 2: 63-72, DOI: 10.25236/AJMC.2025.060209

stratification along the z-direction, resulting in a large velocity gradient. In contrast, the velocity distribution of the LDP and LIP structures is more uniform, with the degree of uniformity following the order: 2SD(I)P < 3SD(I)P < LD(I)P.

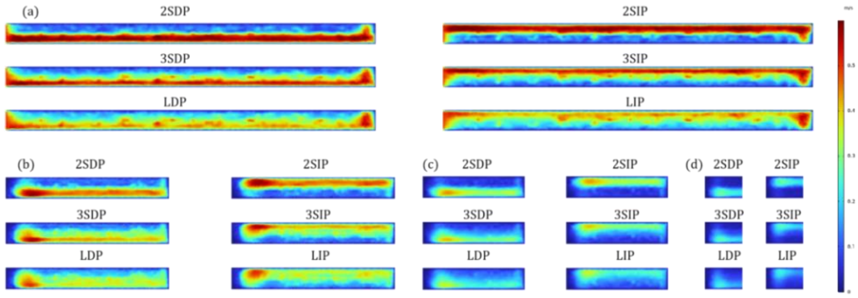

Fig. 6 The velocity distribution at the interface between the gradient porous wall and the channel: (a) Level 0; (b) Level 1; (c) Level 2; (d) Level 3.

3.2 Influence of inlet velocity

As depicted in Figure 7(a), the Nusselt number for several designs exhibits an increasing trend as the inlet velocity increases. And the three models with increasing porosity gradient in the z-direction (2SIP, 3SIP, and LIP) can enhance the Nusselt number. This is because, near the bottom heating source, heat transfer in bifurcated microchannels is primarily governed by heat conduction. At this location, a design with low porosity exhibits a higher proportion of solid skeleton, thereby enhancing its heat conduction capability significantly. However, near the top, it is predominated by convective heat transfer. The designs with high porosity exhibit a high convective heat transfer coefficient between the fluid and the solid, resulting in enhanced heat transfer efficiency. Therefore, the gradient increasing design demonstrates superior effectiveness. It can be observed from Fig. 7(b) that the overall thermal resistance decreases as the inlet velocity increase

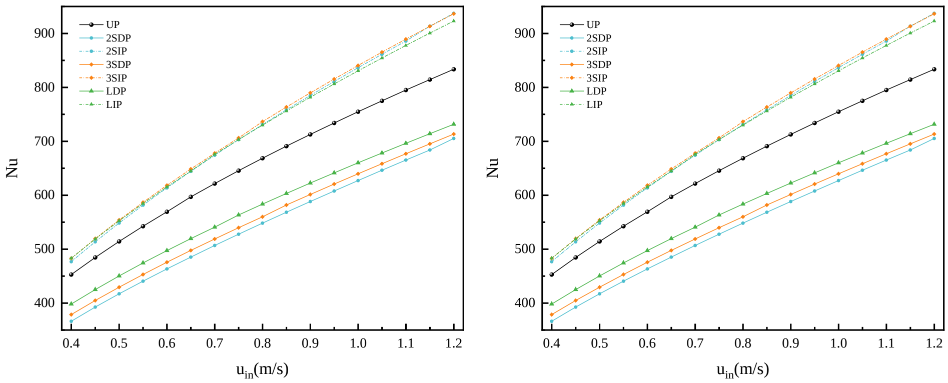

Fig. 7 The (a) Nusselt number and (b) overall thermal resistance of gradient porous walls at different inlet velocity

It can be observed from Fig. 8 that the friction coefficient of the bifurcated microchannel decreases gradually as the inlet velocity increases progressively. Furthermore, the friction coefficients of the six models with gradient porosity walls are all lower than that of the UP model. This demonstrates that the gradient porosity wall can significantly reduce the pressure drop between the inlet and outlet of the bifurcated microchannel, thereby enhancing its hydraulic performance. Among them, two-layer step gradient structures exhibit the lowest friction factor. This is because the SI(D)P structures have the highest proportion of the large porosity porous materials in the whole wall. And the big contact area between the fluid and the solid, coupled with low flow resistance, results in a reduction of pressure throughout the entire system. Where the friction factor of the 2SIP is the lowest, being 6.5% and 3.4% lower than that of the 3SIP and LIP, respectively.

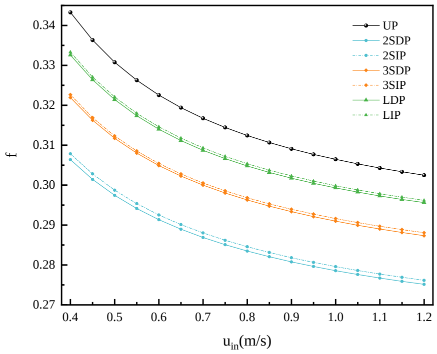

Fig. 8 The effect of inlet velocity on the friction coefficient of gradient porous walls

Based on the preceding analysis, it is evident that the flow performance of structures with a decreasing porosity gradient along the z-direction is superior. Conversely, the thermal performance of structures with an increasing porosity gradient is more favorable. To comprehensively consider both thermal and flow performance, a PEF is introduced, as defined in Equation (3-11). It can be observed from Fig. 9 that the PEF of the structure with an increasing porosity is higher than that of the structure with a decreasing porosity. Moreover, the 2SIP design demonstrates the best overall performance.

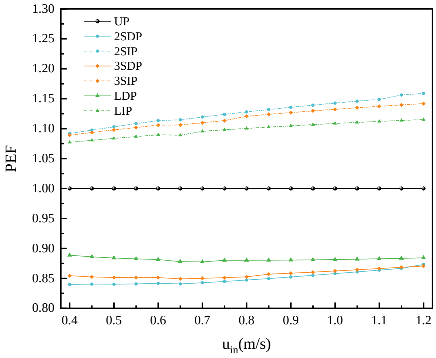

Fig. 9 The influence of inlet velocity on the PEF of gradient porous walls

4. Conclusion

In this study, a novel type of porous wall with a gradient porosity along the z-direction was designed and integrated into the bifurcated microchannel. Additionally, a three dimensional conjugate heat transfer model was developed. The effects of various porosity gradient designs, inlet velocity, and the gradient difference of porosity on the heat transfer, flow, and overall performance were numerically investigated using the finite element method. The key findings are as follows:

(1) The LIP, 2SIP, 3SIP can effectively decrease the local thermal resistance of the bifurcated microchannel. Where the LIP is minimized, achieving a 5% reduction compared to the UP.

(2) When the inlet velocity increases, the Nusselt number rises and the overall thermal resistance decreases. The 2SIP, 3SIP, LIP can significantly enhance the heat transfer capability of the bifurcated microchannels, characterized by a high Nusselt number, low overall thermal resistance, and a large comprehensive performance factor.

In summary, the 2SIP structure demonstrates the best comprehensive performance and contributes to the most significant improvement in overall performance. The gradient porous wall introduced in this study can significantly enhance the flow and heat transfer performance of bifurcated microchannels. It provides a research foundation for the design of MCHS, fuel cell flow channels, and other relevant fields. Furthermore, it facilitates the application of gradient porous materials and other advanced heat transfer enhancement techniques in composite heat transfer systems.

References

[1] Ajeeb W, Murshed S M S. Nanofluids in compact heat exchangers for thermal applications: A State-

of-the-art review. Thermal Science and Engineering Progress, 2022, 30: 101276. https://doi.org/10.1016/j.tsep.2022.101276.

[2] Alihosseini Y, Targhi M Z, Heyhat M M, et al. Effect of a micro heat sink geometric design on thermo-hydraulic performance: A review. Applied Thermal Engineering, 2020, 170: 114974. https://doi.org/10.1016/j.applthermaleng.2020.114974.

[3] Marchetto D B, Ribatski G. An experimental study on flow boiling heat transfer of HFO1336mzz(Z) in microchannels-based polymeric heat sinks. Applied Thermal Engineering, 2020, 180: 115815. https://doi.org/10.1016/j.applthermaleng.2020.115815.

[4] Tuckerman D B, Pease R F W. High-performance heat sinking for VLS. IEEE Electron device letters, 1981, 2(5): 126-129. https://doi.org/10.1109/edl.1981.25367.

[5] Tuckerman D B. Heat-transfer microstructures for integrated circuits (cooling, heat-sink). Stanford University, 1984.

[6] Mandelbrot B B. Is nature fractal? Science, 1998, 279(5352): 783-783. https://doi.org/10.1126/science.279.5352.783c.

[7] Murray C D. The physiological principle of minimum work: I. The vascular system and the cost of blood volume. Proceedings of the National Academy of Sciences, 1926, 12(3): 207-214. https://doi.org/10.1073/pnas.12.3.207.

[8] Murray C D. The physiological principle of minimum work applied to the angle of branching of arteries. The Journal of general physiology, 1926, 9(6): 835. https://doi.org/10.1085/jgp.9.6.835.

[9] Senn S M, Poulikakos D. Laminar mixing, heat transfer and pressure drop in tree-like microchannel nets and their application for thermal management in polymer electrolyte fuel cells. Journal of Power Sources, 2004, 130(1-2): 178-191. https://doi.org/10.1016/j.jpowsour.2003.12.025.

[10] Wang X Q, Mujumdar A S, Yap C. Effect of bifurcation angle in tree-shaped microchannel networks. Journal of Applied Physics, 2007, 102(7): 073530. https://doi.org/10.1063/1.2794379.

[11] Peng Y, Liu W, Wang N, et al. A novel wick structure of vapor chamber based on the fractal architecture of leaf vein. International Journal of Heat and Mass Transfer, 2013, 63: 120-133. https://doi.org/10.1016/j.ijheatmasstransfer.2013.02.021.

[12] Xia C, Fu J, Lai J, et al. Conjugate heat transfer in fractal tree-like channels network heat sink for high-speed motorized spindle cooling. Applied Thermal Engineering, 2015, 90: 1032-1042. https://doi.org/10.1016/j.applthermaleng.2015.07.024.

[13] Zhang Y, Xia Z, Song B, et al. Experimental analysis on the loop heat pipes with different microchannel evaporators. Applied Thermal Engineering, 2020, 178: 115547. https://doi.org/10.1016/j.applthermaleng.2020.115547.

[14] Fang K, Xu S L. Microfludic and heat transfer performance of multilayer fractal-like microchannel network. Advanced Materials Research, 2011, 422: 392-396. https://doi.org/10.4028/www.scientific.net/AMR.422.392.

[15] Yan Y, Yan H, Feng S, et al. Thermal-hydraulic performances and synergy effect between heat and flow distribution in a truncated doubled-layered heat sink with Y-shaped fractal network. International Journal of Heat and Mass Transfer, 2019, 142: 118337. https://doi.org/10.1016/j.ijheatmasstransfer.2019.06.093.

[16] Sam M, Jojith R, Radhika N. Progression in manufacturing of functionally graded materials and impact of thermal treatment—A critical review. Journal of Manufacturing Processes, 2021, 68: 1339-1377. https://doi.org/10.1016/j.jmapro.2021.06.062.

[17] Hu C, Li H, Tang D, et al. Pore-scale investigation on the heat-storage characteristics of phase change material in graded copper foam. Applied Thermal Engineering, 2020, 178: 115609. https://doi.org/10.1016/j.applthermaleng.2020.115609.

[18] Gao X, Wei P, Yu J, et al. Design and assessments on graded metal foam in heat storage tank: An experimental and numerical study. International Communications in Heat and Mass Transfer, 2023, 146: 106902. https://doi.org/10.1016/j.icheatmasstransfer.2023.106902.

[19] Kang D G, Lee D K, Choi J M, et al. Study on the metal foam flow field with porosity gradient in the polymer electrolyte membrane fuel cell. Renewable Energy, 2020, 156: 931-941. https://doi.org/10.1016/j.renene.2020.04.142.

[20] Li M, Zhao Y, Long R, et al. Gradient porosity distribution of adsorbent bed for efficient adsorption cooling. International Journal of Refrigeration, 2021, 128: 153-162. https://doi.org/10.1016/j.ijrefrig.2021.03.013.

[21] Xu Z G, Zhao C Y. Enhanced boiling heat transfer by gradient porous metals in saturated pure water and surfactant solutions. Applied Thermal Engineering, 2016, 100: 68-77. https://doi.org/10.1016/j.applthermaleng.2016.02.016.

[22] Wu M, Shen S, Yang X, et al. Advances in the enhancement of bionic fractal microchannel heat transfer process. Journal of Thermal Analysis and Calorimetry, 2023, 148(23): 13497-13517.

ISSN 2616-5880 Vol. 6, Issue 2: 63-72, DOI: 10.25236/AJMC.2025.060209

https://doi.org/10.1007/s10973-023-12620-4.
[23] Hung T C, Huang Y X, Sheu T S, et al. Numerical optimization of the thermal performance of a porous-microchannel heat sink. Numerical Heat Transfer, Part A: Applications, 2014, 65(5): 419-434. https://doi.org/10.1080/10407782.2013.836005.
[24] Alazmi B, Vafai K. Analysis of variants within the porous media transport models. International Journal of Heat and Mass Transfer, 2000, 122(2): 303-326. https://doi.org/https://doi.org/10. 1115/1.521468.
[25] Nield D A, Bejan A. Convection in porous media. Springer: New York, 2006. https://doi.org/10.1007/978-1-4757-3033-3.
[26] Ghahremannezhad A, Vafai K. Thermal and hydraulic performance enhancement of microchannel heat sinks utilizing porous substrates. International Journal of Heat and Mass Transfer, 2018, 122: 1313-1326. https://doi.org/10.1016/j.ijheatmasstransfer.2018.02.024.
[27] Ergun S. Fluid flow through packed columns. Chemical engineering progress, 1952, 48(2): 89–94. https://doi.org/10.1016/0009-2509(53)80048-5.